

VPUFormer: Visual Prompt Unified Transformer for Interactive Image Segmentation

Xu Zhang, Kailun Yang[†], Jiacheng Lin, Jin Yuan^{*†}, Zhiyong Li^{*}, *Member, IEEE*, and Shutao Li, *Fellow, IEEE*

Abstract—The integration of diverse visual prompts like clicks, scribbles, and boxes in interactive image segmentation could significantly facilitate user interaction as well as improve interaction efficiency. Most existing studies focus on a single type of visual prompt by simply concatenating prompts and images as input for segmentation prediction, which suffers from low-efficiency prompt representation and weak interaction issues. This paper proposes a simple yet effective Visual Prompt Unified Transformer (VPUFormer), which introduces a concise unified prompt representation with deeper interaction to boost the segmentation performance. Specifically, we design a Prompt-unified Encoder (PuE) by using Gaussian mapping to generate a unified one-dimensional vector for click, box, and scribble prompts, which well captures users’ intentions as well as provides a denser representation of user prompts. In addition, we present a Prompt-to-Pixel Contrastive Loss (P²CL) that leverages user feedback to gradually refine candidate semantic features, aiming to bring image semantic features closer to the features that are similar to the user prompt, while pushing away those image semantic features that are dissimilar to the user prompt, thereby correcting results that deviate from expectations. On this basis, our approach injects prompt representations as queries into Dual-cross Merging Attention (DMA) blocks to perform a deeper interaction between image and query inputs. A comprehensive variety of experiments on seven challenging datasets demonstrates that the proposed VPUFormer with PuE, DMA, and P²CL achieves consistent improvements, yielding state-of-the-art segmentation performance. Our code will be made publicly available at <https://github.com/XuZhang1211/VPUFormer>.

Index Terms—Interactive image segmentation, vision transformer, unified prompt representation, contrastive learning.

I. INTRODUCTION

IMAGE segmentation aims to partition an input image into meaningful parts, which is an essential topic in visual scene understanding [1], [2], [3], [4]. The rapid progress of deep learning has significantly promoted the prosperity of interactive image segmentation, which aims at segmenting the desired regions in an image by iteratively inputting visual prompts like scribbles [5], [6], [7], [8], clicks [9], [10], [11], [12], [13], and boxes [14], [15], [16] (see Fig. 1). Most existing approaches first adopt Distance Maps [9] or Disk Maps [17],

X. Zhang, J. Lin, J. Yuan, and Z. Li are with the College of Computer Science and Electronic Engineering, Hunan University, Changsha 410082, China.

K. Yang, Z. Li, and S. Li are with the School of Robotics and the National Engineering Research Center of Robot Visual Perception and Control Technology, Hunan University, Changsha 410082, China.

S. Li is also with the College of Electrical and Information Engineering and with the Key Laboratory of Visual Perception and Artificial Intelligence of Hunan Province, Hunan University, Changsha 410082, China.

^{*}Corresponding authors: Jin Yuan and Zhiyong Li. (E-mail: yuan-jin@hnu.edu.cn, zhiyong.li@hnu.edu.cn.)

[†]Equal advising.

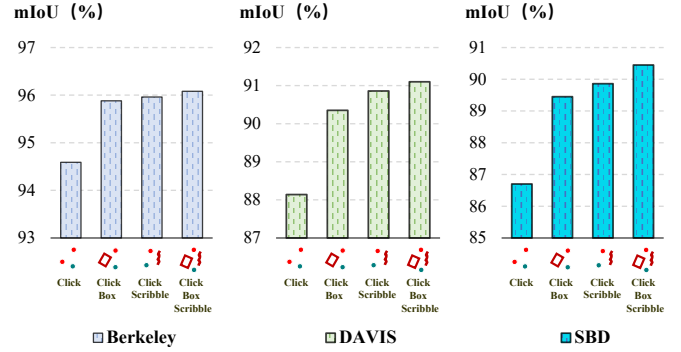


Fig. 1: Performance obtained from the third round of interactive segmentation when using Click alone, and in combination with Box, Scribble, and Box+Scribble (*i.e.*, Click, Click+Box, Click+Scribble, and Click+Box+Scribble). We conduct the evaluations on Berkeley, DAVIS, and SBD datasets.

[18] to represent visual prompts, and then concatenate the prompt maps with the image as input to a segmentation model for instance segmentation. Benefiting from the advances of modeling architecture [19], [20], [21], [22], input representation [12], and loss function [23], [24], interactive image segmentation has achieved impressive performance, which could accurately capture the desired segmentation instances.

In spite of the witnessed success, most existing studies focus on receiving one type of visual prompt during the interaction, which greatly limits users’ behavior and violates their habits. Generally, different visual prompts have different advantages, and allowing a variety of visual prompt inputs is conducive to improving interaction efficiency and offering a flexible interactive interface for users. Therefore, it is crucial to effectively integrate multiple types of visual prompts for enhancing interactive image segmentation.

To represent diverse visual prompts, most approaches simply transform them into coordinate maps by using Disk Map or Distance Map formats [12], which could be simply concatenated with the input image. This paradigm suffers from two problems. First, the 2D sparse representation by Disk Map or Distance Map is inefficient, which not only increases the storage space but also consumes large computation costs. Second, the simple concatenation between image and prompt maps lacks the deep exploration of the correlations between them, thereby being incapable of accurately mapping users’ intentions into the desired segmentation regions.

Towards this end, this paper proposes a simple and effective Visual Prompt Unified Transformer (VPUFormer), which inte-

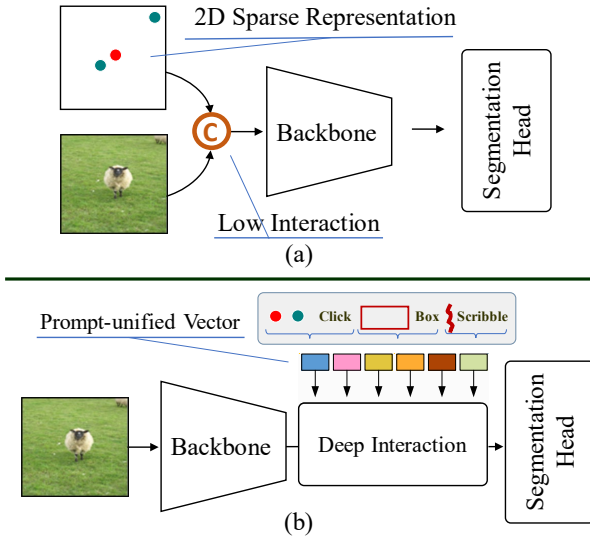


Fig. 2: Comparing the approach of combining user prompts with image inputs and the approach of efficiently interacting with image inputs through user prompts. The former approach suffers from low interaction between user prompts and images, whereas the latter approach implements feature deeper interaction between prompt and image inputs, resulting in more robust feature representations for image segmentation.

grates multiple types of visual prompts including clicks, boxes, and scribbles in a unified format with a deeper interaction for boosting interactive image segmentation performance. Specifically, we design a simple Prompt-unified Encoder (PuE) to offer a unified representation for all the visual prompts. Given a prompt, PuE first generates two one-dimensional vectors in horizontal and vertical directions according to a Gaussian distribution, where the smaller distance to the prompt coordinates represents a higher probability value for the positive or negative property. Then, PuE concatenates the two vectors as the prompt representation. Taking a step beyond Disk Map and Distance Map, our prompt representation is a vector instead of a 2D matrix, which provides a denser representation of user prompts and accurately records spatial location information.

Furthermore, we propose a Prompt-to-Pixel Contrastive Loss (P²CL) that leverages user feedback to gradually refine candidate semantic features. Specifically, P²CL calculates the similarity between user prompt features and image features and utilizes contrastive learning to bring image semantic features closer to the features that are similar to the user prompt, while pushing away those image semantic features that are dissimilar to the user prompt features. By aligning the user prompt features with the corresponding pixel-level visual features, it enables more efficient interaction between the user prompts and images, thereby guiding the model to optimize the expected semantic regions and boundaries effectively. Meanwhile, we design a Dual-cross Merging Attention (DMA) module to strengthen the interaction between query and image inputs. Concretely, DMA first adopts prompt-to-semantic attention to capture notable semantic features guided by prompt queries from images, and semantic-to-prompt attention to

emphasize relative prompt features according to image inputs. Then, DMA concatenates them to generate enhanced features for mask prediction. As shown in Fig. 2, different from simple concatenation, DMA implements feature deeper interaction between prompt and image inputs, thereby generating robust feature representation for interactive image segmentation.

We extensively evaluate our method on seven public benchmarks, and the experimental results demonstrate that the proposed components PuE, DMA, and P²CL are both effective, enabling VPUFormer to yield state-of-the-art performance as compared to existing interactive image segmentation methods. Further, as shown in Fig. 1, our unified approach successfully materializes the advantages of combining multiple prompts and produces consistent performance gains across the datasets. At a glance, the main contributions are summarized as follows:

- We propose a simple and effective Visual Prompt Unified Transformer (VPUFormer) for interactive image segmentation. VPUFormer is featured with Prompt-unified Encoder (PuE) to unify the representations for clicks, boxes, and scribbles, allowing users to input different prompts to be adaptive to complex interactive scenarios. PuE generates a one-dimensional Gaussian vector to provide a denser representation as well as record coordinate information, achieving informative query representations.
- We propose a Prompt-to-Pixel Contrastive Loss (P²CL) to bring image semantic features closer to the features that are similar to the user prompt, while pushing away those image semantic features that are dissimilar to the user prompt features, thereby correcting the previous round of results that did not meet expectations.
- We design a Dual-cross Merging Attention (DMA) module to perform a deeper interaction between image and prompt inputs. DMA adopts prompt-to-semantic and semantic-to-prompt attention to capture notable prompt and visual features, thereby yielding robust feature representation to support mask prediction.
- We evaluate the proposed VPUFormer on seven benchmark datasets. The experimental results prove the effectiveness of the proposed components, yielding state-of-the-art performance for interactive image segmentation.

II. RELATED WORK

A. Interactive Image Segmentation

Early interactive image segmentation approaches mainly adopt optimization-based methods [6] to minimize a specifically constructed cost function defined on a graph over image pixels [15], [25], [26]. Thanks to the advance of deep learning, recent studies have developed a variety of deep learning models for interactive image segmentation [27], [28], [29]. For instance, Xu *et al.* [9] first introduced a deep model to transform positive and negative clicks into separate Euclidean Distance Maps, and then concatenates the maps with an input image as a composite input to a Convolutional Neural Network (CNN) for mask prediction. RITM [12] extends click-based interactive segmentation to allow modifying existing instance segmentation masks interactively, which has inspired numerous subsequent research works in this field. GPCIS [30]

formulates the click-based interactive segmentation task as a pixel-wise binary classification model based on Gaussian processes (GP). It employs amortized variational inference to approximate the GP posterior in a data-driven way and then decouples the approximated GP posterior into dual-space forms for efficient sampling with linear complexity. Besides CNN, transformer-based models are also designed for interactive image segmentation [28], [31], where a user’s clicks are still concatenated with an image as an input to the models for mask prediction. Benefiting from the self-attention mechanism, transformer-based approaches have demonstrated promising performance for interactive image segmentation. This work also adopts transformer-based backbones for interactive image segmentation. Rather than concatenating an image with users’ prompts, our approach separately inputs them into the model with a deep cross-modal interaction to boost the segmentation performance.

B. Different Types of Interactive Feedback

Most interactive image segmentation approaches adopt click prompts as users’ feedback for its simplicity and efficiency [32], [33]. However, since click prompts have a limited receptive field, various works have been devoted to exploring other prompts for interactive feedback. For example, [14] and [16] adopt bounding boxes as feedback queries, which can effectively define the range of a desired region but face uncertainty in region boundaries when dealing with irregular contours. Zhang *et al.* [34] utilized an inside point near the center of an object and two outside points at the symmetrical corners of a tight bounding box to address this limitation, generating extra labeling costs. Besides bounding boxes [14], [15], [16], scribbles [5], [8] are also used for interactive image segmentation, which could provide rich and precise information to capture users’ intentions but requires users to invest more time and knowledge as compared to boxes and clicks. Apart from employing a single form of prompts, several works [35], [36], [37] have explored employing a combination of various forms of prompts for interactive segmentation. For instance, Kirillov *et al.* [36] leveraged learnable vectors with position embeddings to represent various types of prompts. Zou *et al.* [37] constructed a promptable, interactive universal segmentation model, where a visual sampler is used to extract prompt points including clicks, boxes, and scribbles with the corresponding point feature vectors as a user’s feedback. Although unified representations of different visual prompts have been achieved, the above methods require feature mapping or learning of visual prompts and lack deep interaction between visual prompts and images. Beyond them, our approach adopts a simple yet efficient prompt encoding method, which describes visual prompts as a probability distribution with a deep interaction between prompts and images.

C. Iterative Optimization for Local Details

Recent approaches [32], [33] focus on local refinement for interactive image segmentation due to its efficiency and effectiveness. Compared to global refinement, local refinement aims at exploring the differences between the current prediction

and the previous prediction. For instance, FocalClick [32] efficiently updates the mask in the region that the user intends to modify and retains predictions in other regions. Focus-Cut [38] integrates the functions of object segmentation and local refinement. After obtaining the global prediction, it crops click-centered patches from the original image with adaptive scopes to refine the local predictions progressively. FCFI [33] focuses on a local area around the new click and subsequently corrects the feedback based on the similarities of high-level features. It alternately updates and collaboratively refines the feedback and deep features to integrate the feedback into the features. Different from the above approaches, this work explores the deep interaction between prompts and images to guide the model’s optimization for expected region prediction. Moreover, our proposed approach of using deviation-based box prompts achieves the goal of local refinement without increasing the model parameters.

III. VPUFORMER: PROPOSED ARCHITECTURE

A. Overview

Fig. 3 illustrates the architecture of our proposed Visual Prompt Unified Transformer (VPUFormer), which consists of four components: Prompt-unified Encoder (PuE), Image Encoder, Dual-cross Merging Attention (DMA) blocks, and Multi-scale Feature Decoder. Given an image with multiple visual prompts by users, we first employ the PuE to convert multiple types of prompts into a unified representation, as well as use the image decoder to extract the visual feature of the image, respectively. Then, the image and prompt representations are sent to our designed Dual-cross Merging Attention (DMA) blocks, which explore the deep interaction between the representations and generate multi-scale features for mask prediction. Finally, the multi-scale feature decoder upsamples the multi-scale features via the feature pyramid network structure to generate a fusion feature, which is fed into an MLP head to calculate the similarity between prompt features and fusion features by using a Prompt-to-Pixel Contrastive Loss (P^2CL), generating a mask probability map. Different from existing approaches, VPUFormer designs a PuE to better encode visual prompts, and a P^2CL to better align image and prompt features. Moreover, the proposed DMA blocks can deeply explore the correlations between prompt and image inputs, thereby generating robust features for mask generation. Next, we mainly elaborate on PuE, DMA, and P^2CL .

B. Prompt-unified Encoder

As aforementioned, existing works [8], [12], [15] focus on one kind of visual prompt and represent it as a two-dimension sparse map. Differently, the proposed Prompt-unified Encoder (PuE) allows users to flexibly input clicks, boxes, and scribbles for a to-be-segmented image and aims at generating a concise and unified representation for each prompt.

Fig. 4 illustrates the encoding of clicks, boxes, and scribbles by using PuE. To effectively capture a user’s intention, PuE constructs a one-dimension prompt vector q to represent a visual prompt, which is composed of three parts as shown in Fig. 4(a): a horizontal representation vector q_h , a vertical

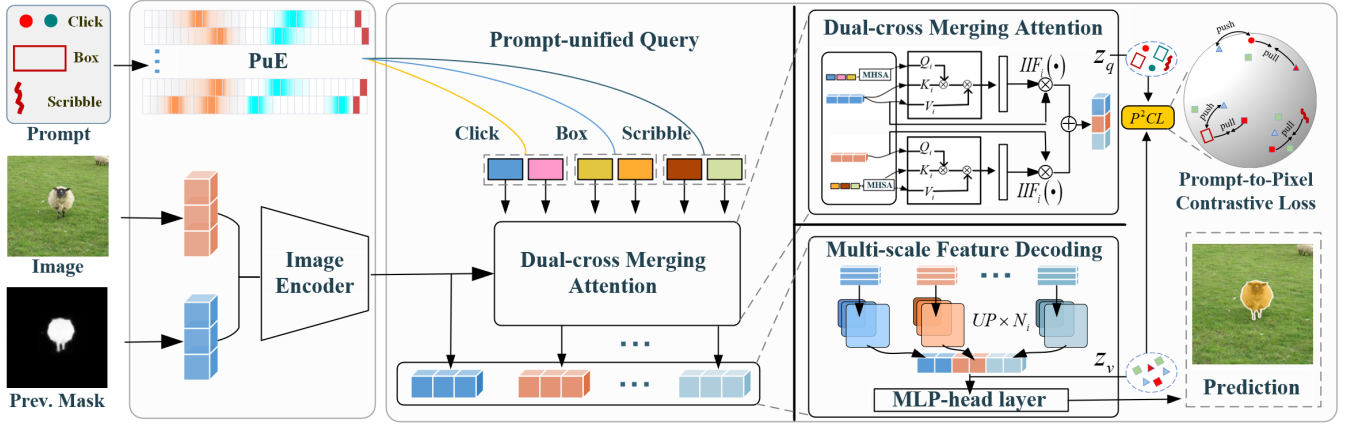


Fig. 3: The pipeline of the proposed Visual Prompt Unified Transformer (VPUFormer). It consists of four components: Prompt-unified Encoder (PuE), Image Encoder, Dual-cross Merging Attention (DMA) blocks, and Multi-scale Feature Decoder.

representation vector q_v , and an intention property bit q_b . The intention property bit records the “positive” (within the desired mask) or “negative” (outside the desired mask) property of a prompt, while the horizontal/vertical representation vector indicates the property probability distribution in the horizontal/vertical direction for the given image according to the prompt. Next, we elaborate on how to encode clicks, boxes, and scribbles, respectively.

Click Encoding. Given a positive/negative click $C_0(x_0, y_0)$ on an image $I \in \mathbb{R}^{H \times W \times 3}$, where H and W are the height and width of I , and (x_0, y_0) is the click’s coordinate. Click encoding aims at generating a horizontal representation vector $q_h \in \mathbb{R}^W$ and a vertical representation vector $q_v \in \mathbb{R}^H$, which reflect the property probability distribution in the horizontal and vertical directions. Taking horizontal representation vector generation as an example, two assumptions are made according to spatial distance and visual distance for property probability estimation. First, if a point has a close spatial distance to x_0 , the probability of them having the same property is high; Second, if a point has a close pixel value as x_0 , which means their visual appearances are similar, then that probability is also high.

Based on the assumptions, given a point $C_i(x_i, y_i)$ in q_h , we first calculate the spatial distance $d_{x_i}^s$ and visual distances $d_{x_i}^v$ between x_i and x_0 as follows:

$$d_{x_i}^s = \sqrt{(x_i - x_0)^2}, i \in [0, W) \quad (1)$$

$$d_{x_i}^v = \sqrt{(p_{x_i} - p_{x_0})^2}, i \in [0, W), \quad (2)$$

where p_{x_i} denotes the pixel value of $C_i(x_i, y_i)$. We then multiply them as the final distance d_{x_i} , which generates a distance vector D_h in the horizontal direction. On this basis, we employ Quasi-Gaussian [39] with a standard deviation σ to convert D_h to a horizontal representation vector q_h as follows:

$$q_h^i = \begin{cases} e^{-\frac{d_{x_i}^2}{2\sigma^2}}, & \text{if } d_{x_i} \leq \sigma \\ 0, & \text{otherwise,} \end{cases} \quad (3)$$

where q_h^i is the i -th element in q_h . In the same way, we can obtain q_v . As shown in Fig. 5, the click encoding vector q_{click} is generated by concatenating q_h , q_v , and q_b as follows:

$$q_{click} = [q_h, q_v, q_b], \quad (4)$$

where $[\cdot]$ is the concatenation operation, and q_b is the one-hot encoding result of “positive” or “negative”.

For all the elements in q_{click} , there are only two elements assigned with the property probability 1, where the first element reflects the horizontal position by $C_0(x_0, y_0)$, and the second indicates the vertical position. Thus, the representation vector q_{click} records the location of a user’s click. Moreover, compared to 2D sparse representation like Disk Map [12], our approach requires less storage and well reflects the property probability distribution for mask prediction.

Box Encoding. Similar to click encoding, box encoding aims at generating horizontal and vertical representation vectors $q_h \in \mathbb{R}^W$ and $q_v \in \mathbb{R}^H$ to reflect the property probability distribution in the horizontal and vertical directions given a box prompt $B_0(x_0, y_0, w_0, h_0)$, where (x_0, y_0) is its center coordinates, and (w_0, h_0) is its width and height. We assume that the center point (x_0, y_0) has the highest probability of satisfying the input property, and a point with a closer distance would have a higher property probability, which is the same as the click encoding. Differently, a box prompt gives the boundary information, which explicitly indicates that the points outside the boundary violate the prompt property. Therefore, we revise Eq. (1) as follows:

$$d_{x_i}^s = \begin{cases} \sqrt{(x_i - x_0)^2} & \text{if } i \in [0, w_0) \\ +\infty, & \text{otherwise.} \end{cases} \quad (5)$$

As a result, the element q_h^i in q_h outside the box would be assigned with zero in Eq. (3). Compared to click encoding, box encoding offers precise boundary information, yielding a better prompt representation vector for mask prediction.

Scribble Encoding. Given a scribble prompt $S(p_0, \dots, p_n)$, where p_0, \dots, p_n denotes the points on the scribble S , we assume the intersection point between $q_h \in \mathbb{R}^W$ and $q_v \in \mathbb{R}^H$ (see Fig. 4(c)) is located at the top-left corner of the scribble

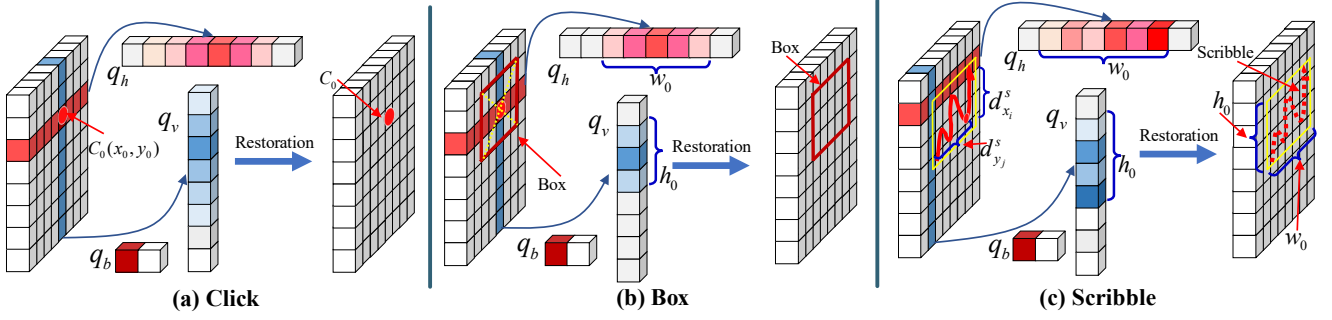


Fig. 4: Three examples to show the click, box, and scribble encoding by the PuE, respectively, where PuE constructs a one-dimension prompt vector q to represent a visual prompt, composing of three parts: a horizontal representation vector q_h , a vertical representation vector q_v , and an intention property bit q_b .

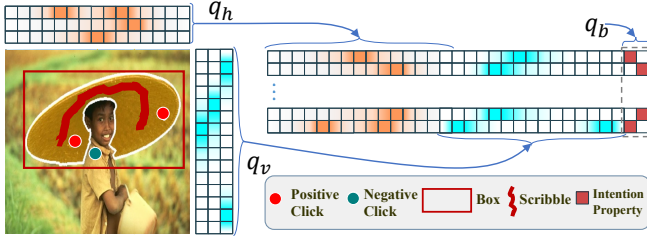


Fig. 5: An example to illustrate the components of the PuE vector by concatenating a horizontal representation vector q_h , a vertical representation vector q_v , and an intention property bit q_b .

bounding box, and the closer a point on q_h/q_v is to the scribble, the higher property probability it is. However, different from clicks and boxes, a scribble is usually an irregular curve composed of continuous points, whose number greatly exceeds the number of elements in q_h and q_v , posing great challenges for scribble encoding.

To tackle this issue, we adopt an approximate strategy to discretize the continuous scribble into a finite number of points $m = (w_0 + h_0)$, where w_0 and h_0 represent the width and height of the bounding box of the scribble. Concretely, as shown in Fig. 4(c), given a point in q_h or q_v , our approach first randomly selects one of the aligned points from the scribble as the candidate. Then, we adopt the click encoding strategy to calculate the distance between the point and the candidate and convert the distance into a property probability.

Different from click and box encoding, scribble encoding only records partial points on a scribble to approximately preserve the contour information of the scribble, resulting in a certain amount of information loss. Nonetheless, scribble encoding offers sufficient information to capture users' intentions to improve the segmentation results. As shown in Algorithm 1, taking horizontal representation vector generation as an example, given a point $p_i(x_i, y_i)$ in q_h and a horizontal alignment point $q_i(x_i, y_i^{q_h})$ on the scribble, we can calculate the distance $d_{x_i}^s$ between them as follows:

$$d_{x_i}^s = \begin{cases} \sqrt{(y_i - y_i^{q_h})^2}, & \text{if } x_i \in [0, w_0) \\ +\infty, & \text{otherwise.} \end{cases} \quad (6)$$

Algorithm 1 Scribble encoding

Input: Scribble $S(p_0, \dots, p_n)$, where p_0, \dots, p_n are points on the scribble;

- 1: Set box $B(x_0, y_0, w_0, h_0)$ the bounding box of the scribble, where (x_0, y_0) is the center point of the box, w_0, h_0 are the width, height of the box, respectively;
- 2: $S(p_0, \dots, p_n)$ discretizes into N points, $N \leq (w_0 + h_0)$;
- 3: Initialization: horizontal/vertical vector $q_h \in \mathbb{R}^W$, $q_v \in \mathbb{R}^H$, and the one-hot encoding label q_b ;
- 4: **for** $x_i = 0$ to w_0 **do**
- 5: $p_i(x_i, y_i) \leftarrow$ randomly select from $p_i(x_i, y_i^0 : y_i^m)$
- 6: $y_i^{q_h} \leftarrow$ the y -axis coordinate of point $p_i(x_i, y_i)$ projected onto the horizontal vector q_h
- 7: Do not select if y_i does not exist
- 8: $d_{x_i}^s = \sqrt{(y_i - y_i^{q_h})^2}$
- 9: $q_i^h = e^{-\frac{d_{x_i}^s}{2\sigma^2}}$ if $d_{x_i}^s \leq \sigma$, else $q_i^h = 0$
- 10: Remove point $p_i(x_i, y_i)$ from $S(p_0, \dots, p_n)$
- 11: **end for**
- 12: **for** $y_j = 0$ to h_0 **do**
- 13: $p_j(x_j, y_j) \leftarrow$ randomly select from $p_j(x_j^0 : x_j^n, y_j)$
- 14: $x_j^{q_v} \leftarrow$ the x -axis coordinate of point $p_j(x_j, y_j)$ projected onto the vertical vector q_v
- 15: Do not select if x_j does not exist
- 16: $d_{y_j}^s = \sqrt{(x_j - x_j^{q_v})^2}$
- 17: $q_j^v = e^{-\frac{d_{y_j}^s}{2\sigma^2}}$ if $d_{y_j}^s \leq \sigma$, else $q_j^v = 0$
- 18: **end for**
- 19: $q_{scribble} \leftarrow$ concatenate q_h, q_v, q_b

Output: $q_{scribble}$

Then, we further convert the distance vector D_h into a probability distribution by using Eq. (3). Scribble Encoding uses $\frac{m}{n}$ points on a scribble with a certain information loss to capture a user's intention, which could preserve the contour information of a scribble to some extent.

In summary, the proposed PuE allows users to flexibly input visual prompts, and could efficiently integrate valuable visual cues for interactive image segmentation, offering concise and dense prompt representations for mask prediction.

C. Dual-cross Merging Attention

Dual-cross Merging Attention (DMA) aims to select informative features that exhibit the highest mutual response between prompt and image features, which consists of a multi-head self-attention layer, two multi-head cross-modal attention layers, two feed-forward neural layers, and an interactive information filtering layer (see Fig. 3).

Concretely, given a prompt feature q and a visual feature f_v as an input, DMA first passes q into a Multi-Head Self-Attention (MHSA) layer to obtain the feature q' , which highlights the important areas in $I \in \mathbb{R}^{3 \times H \times W}$. On this basis, the Multi-Head Cross-modal Attention (MHCA) layer [40] performs the cross-modal attention on q' and f_v to generate the prompt-to-semantic feature F_{qv} and the semantic-to-prompt feature F_{vq} , respectively. These features are then passed through two Feed-Forward Neural (FFN) layers:

$$\begin{aligned} F_{qv} &= \text{MHCA}(q', f_v, f_v) + q, \\ F_{vq} &= \text{MHCA}(f_v, q', q') + f_v, \end{aligned} \quad (7)$$

$$\begin{aligned} \hat{F}_{qv} &= \text{FFN}(\text{LN}(F_{qv})), \\ \hat{F}_{vq} &= \text{FFN}(\text{LN}(F_{vq})), \end{aligned} \quad (8)$$

where F_{qv} and F_{vq} represent the cross-attention features from q' to f_v and from f_v to q' , respectively, and $\text{LN}(\cdot)$ denotes layer normalization. Subsequently, they are fed into an Interactive Information Filtering (IIF) layer to calculate the interactive response and select the feature with the highest interactive response value for each prompt channel. In detail, we use the Sigmoid function to obtain the interactive weights, and these weights are then element-wise multiplied with the visual features to obtain \hat{F}_{iqv} and \hat{F}_{ivq} respectively, which helps to select effective interactive information based on user prompts and filter out invalid and redundant information:

$$\begin{aligned} \hat{F}_{iqv} &= \text{IIF}(\hat{F}_{qv}, f_v) = \text{Sigmoid}(\phi(\hat{F}_{qv})) \otimes f_v, \\ \hat{F}_{ivq} &= \text{IIF}(\hat{F}_{vq}, f_v) = \text{Sigmoid}(\phi(\hat{F}_{vq})) \otimes f_v, \end{aligned} \quad (9)$$

where $\phi(\cdot)$ is an operation that selects the highest interactive response value from \hat{F}_{qv} or \hat{F}_{vq} . Finally, the bidirectional effective interaction feature F_{dual} is formalized as follows:

$$F_{dual} = f_v \times (1 + F_{iqv} + F_{ivq}). \quad (10)$$

For implementation, we use three Dual-Cross Merging Attention (DMA) layers and add the positional encodings [36] to the visual features. In addition, all the original prompt features are re-added as the query feature inputs of each layer to obtain stronger prompt clues.

D. Multi-scale Feature Decoder

To capture rich multi-scale spatial information, we adapt a feature pyramid that is commonly produced by an FPN [41] to combine features from different stages. Firstly, we use $4 \times$ upsampling with two transposed convolutional layers to upsample the bidirectional interactive features F_{dual} output by each dual-cross merging attention layer (obtaining feature resolutions relative to the input image of $1/4$, $1/16$, $1/32$, and $1/64$, respectively) as follows:

$$F_m^i = \text{UP}_{\times \Delta_i}(F_{dual}^i), \Delta \in \{4, 16, 32, 64\}, i \in [1, 4], \quad (11)$$

where $\text{UP}(\cdot)$ denotes the upsampling operation and $\{4, 16, 32, 64\}$ represent the upsampling factors. F_{dual}^i represents the output of the i -th dual-cross merging attention layer. Subsequently, the multi-scale features are transformed to have an identical channel dimension by passing through a 1×1 convolutional layer and then are upsampled with the same resolution for concatenation. Finally, the concatenated features are passed through an MLP-head layer to output a single-channel feature, which is through a sigmoid function to obtain a segmentation probability map. The MLP-head layer only uses a 1×1 convolutional layer.

$$\hat{F}_m^i = \text{Conv}(F_m^i), \quad (12)$$

$$\hat{F}_v = [\hat{F}_m^1, \hat{F}_m^2, \hat{F}_m^3, \hat{F}_m^4], \quad (13)$$

where $[\cdot]$ denotes the concatenation operation and $\text{Conv}()$ denotes a 2D 1×1 convolution.

E. Prompt-to-Pixel Contrastive Loss (P^2CL)

Interactive user prompts aim to progressively reduce uncertainty among numerous potential semantics while guiding and filtering the features that align with the user's expectations. Prior methods have overlooked this aspect, leading to a lack of consistency between user intentions and visual concepts in the image. To tackle this issue, we design a prompt-to-pixel contrastive loss, which explicitly aligns the user prompt features with the corresponding pixel-level visual features. Concretely, we first align the dimensions of \hat{F}_v with q' , and then normalize the transformed \hat{F}_v and q' as follows:

$$\begin{aligned} z_v &= \text{normalize}(\hat{F}_v), \\ z_q &= \text{normalize}(q'W_q + b_q), \end{aligned} \quad (14)$$

where $z_v \in \mathbb{R}^{\frac{H}{4} \times \frac{W}{4} \times D}$, $z_q \in \mathbb{R}^{N \times D}$ are the representations of \hat{F}_v and q' in the new space, N denotes the number of user interactions, W_q is the learnable matrix to transform q' into the feature dimension D , and b_q is the learnable bias term. Next, we calculate the similarity between z_q and z_v through a dot product operation as follows:

$$\rho = \frac{1}{2}(z_q \cdot z_v^\top + 1), \quad (15)$$

where $\rho \in \mathbb{R}^{N \times \frac{H}{4} \times \frac{W}{4}}$ indicates the similarity between them. Finally, for each element i in z_q and j in z_v , we calculate its prompt-to-pixel loss as follows:

$$\text{P}^2\text{CL}(z_q^i, z_v^j) = \begin{cases} -\log(\rho_{i,j}), & Y_{i,j} \in \mathcal{P}, \\ -\log(1 - \rho_{i,j}), & Y_{i,j} \in \mathcal{N}, \end{cases} \quad (16)$$

where \mathcal{P} and \mathcal{N} denote positive and negative pixel sets in the ground truth, and $Y_{i,j}$ represents the j -th ground-truth label located on the mask corresponding to the i -th interaction. The P^2CL loss function is expressed as:

$$\ell_{\text{P}^2\text{CL}} = \frac{1}{N \times L} \sum_{i=0}^{N-1} \sum_{j=0}^{L-1} \text{P}^2\text{CL}(z_q^i, z_v^j), \quad (17)$$

where $L = \frac{H}{4} \times \frac{W}{4}$ is the flatten length. The P^2CL loss can well pull features closer between the representations of positive prompts and the corresponding image features, as well

as push away the negative elements. As a result, the mapping feature better reflects a user’s intention to capture the desired segmentation mask.

Finally, the total loss is calculated as the sum of the NFL loss [12], DICE loss [42], and the proposed P²CL loss:

$$\mathbb{L}_{\text{total}} = \ell_{\text{NFL}} + \ell_{\text{DICE}} + \lambda \ell_{\text{P}^2\text{CL}}, \quad (18)$$

where λ is a hyperparameter to adjust the scale of $\ell_{\text{P}^2\text{CL}}$.

IV. EXPERIMENTS

In this section, we first introduce our datasets and experimental settings, followed by the illustration of experimental results with detailed analyses.

A. Datasets

We conduct experiments on seven public datasets including four natural datasets and three medical datasets.

Training Sets. We use the following two training datasets.

- SBD [44]: This dataset contains 8,498 images for training, which is widely used as a training dataset for the interactive image segmentation task.
- COCO [48]+LVIS [49]: COCO contains 118K training images (with a total of 1.2M instances), and LVIS shares the same images with COCO but has more instance masks and higher mask quality.

Testing Sets. We use the following six testing datasets to evaluate our model.

- GrabCut [15]: It contains 50 images with 50 instances, and each image has clear foreground and background differences.
- Berkeley [43]: This dataset includes 96 images with 100 instances in the validation set, which is used for evaluation in our experiments.
- SBD [44]: This dataset contains 2,857 validation images with 6,671 instances. Following [12], [32], [38], we evaluate our model on the validation dataset.
- DAVIS [45]: This dataset contains 50 videos, and we only use the same 345 frames as used in [28], [32], [38], [50] for evaluation.
- ssTEM [51]: It includes two image stacks, and each contains 20 medical images. We evaluate our model on the same stack as used in [52] for evaluation.
- BraTS [53]: This dataset includes 369 Magnetic Resonance Image (MRI) volumes, and we use the same 369 slices as used in [52].
- OAIZIB [54]: This dataset contains 507 MRI volumes, and we test on the same 150 slices with 300 instances as used in [52].

Evaluation Metrics. We evaluate our model by using the standard Number of Clicks (NoC) metric, which measures the number of clicks required to achieve a predefined Intersection over the Union (IoU) threshold between predicted and ground truth masks. We denote NoC with the IoU threshold set to 85% and 90% as NoC@85 and NoC@90, respectively. The maximum number of clicks for each instance is set to 20. The Number of Failures (NoF) is also reported and it counts

the number of images that cannot achieve the target IoU within the specified maximum number of clicks. Besides, we use the average IoU given k clicks (IoU@ k) to evaluate the segmentation quality given a fixed number of clicks.

B. Implementation Details

To demonstrate the generality of our method, we conduct experiments under four backbones: ViT-B [19], SegFormerB0-S2 [22], HRNet18s [21], and DeepLabV3+ [55] with ResNet50 [20]. For image input, all the input images are unified to the size of 448×448 , and the prompts are encoded into a Gaussian vector with $\sigma=3$. Data augmentation techniques, including random resizing (scale ranges from 0.75 to 1.25), random flipping and rotation, random brightness contrast, and random cropping, are used to boost performance. Additionally, we input the previous forward-pass predicted mask $M \in \mathbb{R}^{1 \times H \times W}$ to the model. Following previous works [12], [47], we employ a Conv1S network architecture to fuse the predicted mask and image. To train our model, the initial learning rate is 5×10^{-4} for SegFormerB0-S2, ResNet50, and HRNet18s, and 5×10^{-5} for ViT-B. The learning rate is then reduced by a factor of 0.1 after 50 epochs. The Normalized Focal Loss (NFL) [12] is used during training with $\alpha=0.5$ and $\gamma=2$. We train our model for 55 epochs by using the Adam optimizer ($\beta_1=0.9$ and $\beta_2=0.999$) with a batch size of 32. All of our models are trained on two NVIDIA RTX A6000 GPUs.

Iterative Sampling Strategy. To better simulate users’ habits, we iteratively add one of the prompts into the model as follows: For training, three different prompts are randomly fed into the model in an iterative manner. During the evaluation, we use only one specific prompt or alternate between multiple prompts. We evaluate the model performance in three scenarios: using a single prompt type, combining click and box or scribble prompts, and using all three prompt types together. Concretely, when using a single prompt type, we keep the prompt input type fixed for performance evaluation. When using two or three prompt types, we first use a click prompt to obtain an initial result. If the IoU is less than the specified threshold $\theta=0.85$ or the improvement between two neighboring iterations is less than 0.05, we randomly switch to box or scribble prompts for boosting performance.

Prompt Simulation Sampling. When starting from a previous mask, we first calculate the False Positive (FP) and False Negative (FN) regions. Similar to the click-based protocol [12], [32], we calculate the max error regions and generate a next prompt from those regions.

C. Experimental Results

1) *Comparison with State-of-the-Art Approaches:* Table I and Table II present the performance analysis of VPU-Former and state-of-the-art methods on GrabCut [15], Berkeley [43], SBD [44], and DAVIS [45] datasets, using SBD and COCO+LVIS as training datasets, respectively. As shown in Table I and Table II, our method demonstrates strong generalization performance across multiple datasets and different backbone architectures. Compared to the previous methods,

TABLE I: Evaluation results on GrabCut [15], Berkeley [43], SBD [44], and DAVIS [45] datasets when the model is trained on the SBD dataset [44]. Throughout this paper, the best and the second-best results for different mainstream backbones are denoted in **bold** and underlined, respectively.

Method	Backbone	GrabCut		Berkeley		SBD		DAVIS	
		NoC@85	NoC@90	NoC@85	NoC@90	NoC@85	NoC@90	NoC@85	NoC@90
RITM [12]	SegFormerB0-S2	1.62	1.82	<u>1.84</u>	2.92	4.26	6.38	4.65	6.13
FocalClick [32]		1.66	1.90	-	3.14	4.34	6.51	5.02	7.06
GPCIS [30]		1.60	<u>1.76</u>	1.84	2.7	4.16	6.28	4.45	6.04
VPUFormer (ours)		1.54	1.68	1.87	2.53	4.10	5.96	4.24	5.78
f-BRS-B [28]	ResNet50	2.20	2.64	2.17	4.22	4.55	7.45	5.44	7.81
CDNet [10]		2.22	2.64	-	3.69	4.37	7.87	5.17	6.66
RITM [12]		2.16	2.3	1.9	2.95	3.97	5.92	4.56	6.05
FocusCut [38]		<u>1.60</u>	1.78	1.86	3.44	3.62	<u>5.66</u>	5	6.38
FocalClick [32]		1.92	2.14	1.87	2.86	3.84	5.82	4.61	6.01
GPCIS [30]		1.64	<u>1.82</u>	<u>1.60</u>	<u>2.60</u>	<u>3.80</u>	5.71	<u>4.37</u>	<u>5.89</u>
VPUFormer (ours)		1.58	1.86	1.52	2.39	3.72	5.60	3.94	5.64
RITM [12]		HRNet-18s	2.00	2.24	2.13	3.19	4.29	6.36	4.89
FocalClick [32]	1.86		2.06	-	3.14	4.3	6.52	4.92	6.48
GPCIS [30]	<u>1.74</u>		<u>1.94</u>	<u>1.83</u>	2.65	<u>4.28</u>	<u>6.25</u>	4.62	<u>6.16</u>
VPUFormer (ours)	1.65		1.82	1.80	<u>2.68</u>	4.12	5.87	<u>4.75</u>	6.13

TABLE II: Evaluation results on the GrabCut [15], Berkeley [43], SBD [44], and DAVIS [45] datasets when the model is trained on COCO + LIVS dataset. “*” denotes that the model is a universal image segmentation model. We reference their accuracy in the interactive image segmentation task.

Method	Backbone	GrabCut		Berkeley		SBD		DAVIS	
		NoC@85	NoC@90	NoC@85	NoC@90	NoC@85	NoC@90	NoC@85	NoC@90
RITM [12]	HRNet-18s	1.54	1.68	-	2.60	4.26	6.86	4.79	6.00
FCFI [33]		<u>1.50</u>	1.56	-	<u>2.05</u>	<u>3.88</u>	<u>6.24</u>	3.70	<u>5.16</u>
VPUFormer (ours)		1.46	<u>1.59</u>	-	1.94	3.76	6.12	<u>3.91</u>	5.08
* SAM [36]	ViT-B	-	-	-	-	6.50	9.76	-	-
* SEEM [37]		-	-	-	-	6.67	9.99	-	-
InterFormer [46]		1.38	1.50	1.99	3.14	3.78	6.34	4.10	6.19
SimpleClick [47]		<u>1.38</u>	<u>1.48</u>	1.36	<u>1.97</u>	<u>3.43</u>	<u>5.62</u>	<u>3.66</u>	<u>5.06</u>
VPUFormer (ours)		1.34	1.40	<u>1.38</u>	1.71	3.32	5.45	3.48	4.82

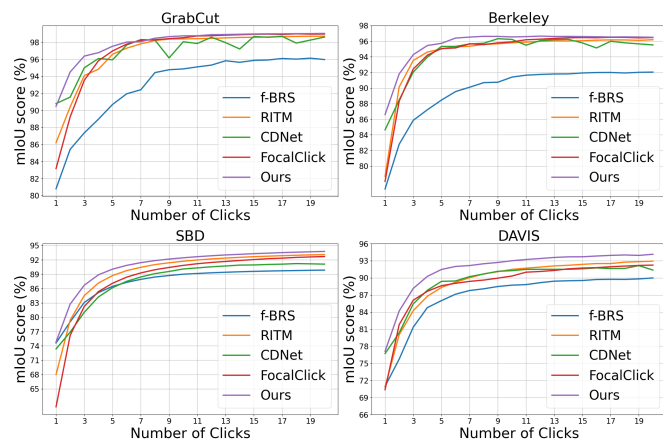


Fig. 6: Comparisons of the mIoU-NoC curves on four datasets.

our approach requires fewer user clicks to achieve 85% and 90% IoU. Moreover, it outperforms previous works in terms of boundary quality. These results highlight the effectiveness of our method in producing accurate segmentation results with reduced user involvement.

Fig. 6 illustrates the mIoU-NoC line charts on four different datasets. The results demonstrate that our approach yields

better results with fewer clicks compared to previous methods. Specifically, the first five clicks of our approach achieve significant improvement over other methods on the GrabCut, Berkeley, and SBD datasets. Furthermore, with additional clicks, our approach eventually converges to better results on all four datasets. Fig. 7 illustrates the quantitative results of our method and some previous methods. In the first column, the mask for the person-object combination is displayed. Due to limited information provided in the first click, all four methods only segmented the person swinging the club while ignoring the golf club. In the second column, during the fifth click, although the other three methods selected the club in subsequent clicks, they still failed to segment the club accurately. Our method successfully segments the complete golf club based on the click prompts on the club. Furthermore, our method achieved the highest IoU on both the initial click and the fifth click. In the third column, when faced with the scenario of foreground regions similar to the background, the other three methods may lose some of the horn regions or mix the background with the horn region. In contrast, our method effectively distinguished the foreground and background based on their semantic attributes in the initial click, resulting in accurate segmentation of the object mask. Moreover, our method further optimized the details in the fifth click. The

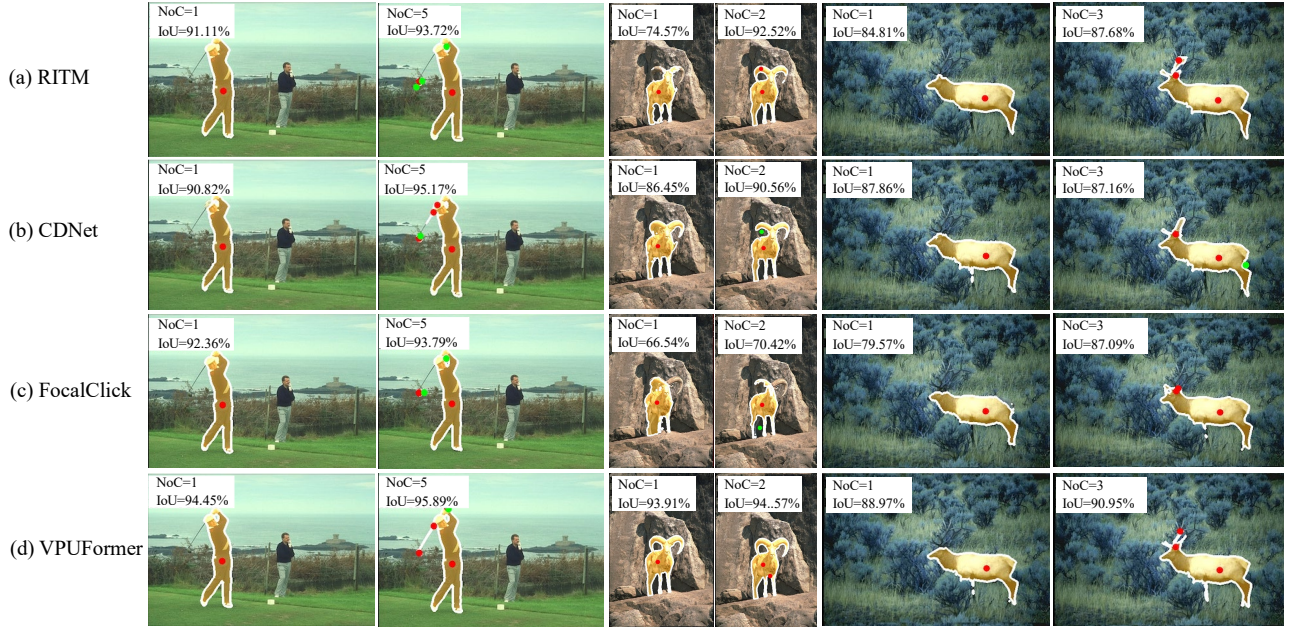


Fig. 7: Qualitative comparisons of RITM [12], CDNet [10], FocusClick [32], and our method. The first two columns show the mask of the combination of people and objects, the middle two columns demonstrate cases where foreground regions are similar to the background and the last two columns show cases where the foreground and background regions are similar, while target regions are partially occluded. Our proposed method can effectively deal with the failures of other methods in the scenarios of multi-object co-segmentation, complex color backgrounds, and object occlusions.

TABLE III: Comparison in NoC@85 and NoC@90 between VPUFormer and state-of-the-art methods trained on the COCO+LVIS dataset and tested on ssTEM, BraTS, and OAIZIB datasets.

Method	Backbone	ssTEM		BraTS		OAIZIB	
		NoC@85	NoC@90	NoC@85	NoC@90	NoC@85	NoC@90
CDNet [10]	ResNet-34	4.15	8.45	10.51	14.80	17.42	19.81
RITM [12]	HRNet32	<u>2.74</u>	<u>4.06</u>	<u>7.56</u>	<u>11.24</u>	15.89	19.27
FocalClick [32]	SegF-B3	3.95	5.05	7.17	11.19	12.93	19.23
SimpleClick [47]	ViT-B	4.25	5.61	8.25	11.83	15.57	<u>18.98</u>
VPUFormer (ours)	ViT-B	2.64	3.90	7.89	11.73	<u>14.97</u>	18.94

fifth and sixth columns show cases where the foreground and background regions are similar, while certain parts of the target object are occluded. It can be seen that all four methods cannot segment the antlers and occluded parts of the front legs during the first click. However, through iterative clicks, our method successfully segments the antlers and occluded parts of the front legs by the fifth click, whereas the other three methods still cannot well handle this situation.

To evaluate the generalizability of our proposed method, we conduct experiments on three medical image datasets: ssTEM [51], BraTS [53], and OAIZIB [54]. Table III reports the evaluation results on these three datasets. We directly apply our models trained on COCO+LVIS datasets to the medical images without fine-tuning. Representative qualitative results on the three medical datasets are shown in Fig. 8. It becomes evident that the segmentation results of the first click on these medical datasets are lower than those of natural datasets. Specifically, there is a significant drop in performance on the

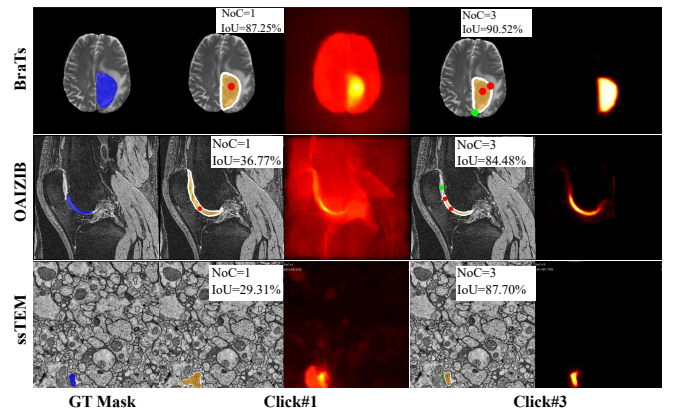


Fig. 8: Visualization results on three medical datasets: BraTS, OAIZIB, and ssTEM.

OAIZIB and ssTEM datasets, which may be due to the target ambiguity in the images, where many target masks overlap and are difficult to determine with a single click. However, we observe a substantial improvement in the segmented regions after the third click, as our VPUFormer enhances the interaction between user intention and image by utilizing the newly provided prompt information, thereby reducing uncertainty in object localization. Overall, this experiment demonstrates that our proposed method can generalize well to medical images and effectively alleviate the problem of target ambiguity.

2) *Ablation Study*: We conduct experiments to verify that PuE can better encode visual prompts compared to the Distance map and the Learning vector methods. The Distance

TABLE IV: Ablation study of different ways of feeding user prompts to the network trained on the COCO+LVIS dataset and tested on Berkeley [43] and DAVIS [45] datasets.

Encoding Type	Berkeley		DAVIS	
	NoC@85	NoC@90	NoC@85	NoC@90
Distance map	1.57	2.20	3.83	5.27
Learning vector	1.43	1.96	3.62	5.08
PuE vector	1.38	1.71	3.48	4.82

TABLE V: Performance comparison of VPUFormer with different components on Berkeley [43] and DAVIS [45] datasets.

Backbone	Method		Berkeley		DAVIS	
	DMA	P ² CL	NoC@90	NoF ₂₀ @90	NoC@90	NoF ₂₀ @90
HRNet-18s	-	-	2.53	6	5.53	78
	✓	-	2.28	3	5.25	61
	-	✓	2.16	2	5.37	58
	✓	✓	1.94	1	5.08	56
ViT-B	-	-	2.46	2	5.48	56
	✓	-	1.92	1	5.26	51
	-	✓	2.13	1	5.12	49
	✓	✓	1.71	0	4.82	48

map represents the user prompt encoded using the Distance map method, while the Learning vector represents the user prompt transformed into a learnable embedding vector using clicks, bounding boxes, or scribbles as input. The PuE vector represents the use of the PuE method to encode the user prompt. From Table IV, we can draw the following conclusions: (a) Using PuE as network input significantly improves performance, with PuE achieving the best NoC@85 and NoC@90 on Berkeley and DAVIS datasets. Compared to the other two methods, the NoC@90 on Berkeley decreases from 2.20 and 1.96 to 1.71, and on DAVIS decreases from 5.27 and 5.08 to 4.82. This suggests that PuE generates one-dimensional Gaussian vectors to capture user intentions and record coordinate information, which leads to informative query representations. In contrast, the Distance map method maps the prompt to a one-dimensional vector as the transformer input, achieving the worst NoC@90 on Berkeley and DAVIS datasets. We speculate this is due to the loss of spatial correlation and positional information during the conversion to a one-dimensional vector. (b) On the Berkeley and DAVIS datasets, the performance of the learning vector method is between the Distance map method and the PuE method. This indicates that the learning vector method performs better than the Distance map method, but it fails to capture salient features effectively due to the lack of deeper interaction between the user prompt and the image. Thus, it achieves lower NoC@90 than the PuE method on Berkeley and DAVIS datasets.

We compare three architecture variants, namely, without using the transformer structure (baseline), Dual-cross Merging Attention (DMA), and Prompt-to-Pixel Contrastive Loss (P²CL) on Berkeley and DAVIS. As shown in Table V, when embedding a single module (DMA or P²CL), the model performance is improved. The DMA module showed greater performance improvement, indicating that the Dual-

TABLE VI: The impact of hyperparameter settings on VPUFormer. We train our model on the COCO+LVIS dataset [44] and test on Berkeley [43] and DAVIS [45] datasets.

λ	Berkeley		DAVIS	
	NoC@85	NoC@90	NoC@85	NoC@90
0	1.45	1.92	3.81	5.26
0.1	1.43	1.76	3.76	5.10
0.5	1.41	1.66	3.94	5.18
1	1.37	1.68	3.70	5.03
2	1.38	1.71	3.48	4.82
5	1.45	1.72	3.92	5.12

Cross merging attention module enhances effective interaction between user prompts and input images, thus promoting segmentation performance. The P²CL module also improves the results, demonstrating that by aligning the user prompt features with the corresponding pixel-level visual features, candidate semantic features can be gradually refined. On NoF@90, the P²CL shows fewer failures in achieving the specified IoU compared to the baseline and DMA. This improvement is attributed to P²CL utilizing user feedback to correct results that deviate from expectations. When both modules are combined, our method achieves significant reductions in the Number of Clicks (NoC) and the Number of Failures (NoF), which verifies the effectiveness of the proposed components.

To investigate the impact of P²CL on model performance, we adjust the weight of P²CL in model optimization by setting different λ values. In Table VI, the hyperparameter λ is set in the range of [0, 5]. We can observe that when λ is set to 0 (*i.e.*, without using P²CL), the performance is the worst on NoC@90 on the Berkeley and DAVIS datasets. As λ increases to 2, the best results are achieved on NoC@85 and NoC@90 on the DAVIS dataset, and close to the best results on NoC@85 and NoC@90 on the Berkeley dataset (with λ values of 1 and 0.5, respectively). However, when λ further increases to 5, the performance of the model decreases on both the Berkeley and DAVIS datasets. The experimental results demonstrate that P²CL brings benefits to the model performance, and the overall best performance is achieved when λ is set to 2.

We conduct ablation experiments to quantitatively analyze the impact of combining different types of user prompts on model performance. From Table VII, it can be observed that the performance is lowest when using Click alone compared to other combinations on both datasets. When combining Click with Box, there is a significant improvement in performance on both Berkeley and DAVIS datasets. The NoI@90 on the Berkeley and DAVIS datasets improves from 1.71 and 4.82 to 1.67 and 4.65, respectively. Similar gains are observed when combining Click with Scribble. When combining three types of feedback for the segmentation task, there is a further improvement in NoI@90 on Berkeley and DAVIS datasets compared to using two types of feedback. This indicates that using multiple types of feedback in interactive segmentation tasks can provide richer information compared to using only click. Furthermore, as different types of interactive feedback are incorporated, their respective advantages can be effectively exploited, thereby addressing the issue of insufficient informa-

TABLE VII: Ablation study combining different types of user prompts for evaluation. All models are trained on the COCO+LVIS dataset and tested on Berkeley [43] and DAVIS [45] datasets. “NoI@85/90” denotes the average Number of Interactions (clicks, boxes, or scribbles) required to reach IoU of 85/90%.

Click	Box	Scribble	Berkeley		DAVIS	
			NoI@85	NoI@90	NoI@85	NoI@90
✓	-	-	1.38	1.71	3.48	4.82
✓	✓	-	1.14	1.67	3.01	4.65
✓	-	✓	1.10	1.65	3.06	4.62
✓	✓	✓	1.10	1.59	2.94	4.57

tion from single feedback in complex scenarios.

Comparing the visualization effects of interactive segmentation for three different types of user prompts is illustrated in Fig. 9, by comparing the interactive segmentation effects of three different prompt types, it can be seen that using clicks alone, regardless of the initial or third interaction, the obtained IoU is the lowest among the three types. This is because the information provided by a single click is not sufficient, leading to uncertainty in the semantics to be segmented. From Fig. 9(b) and Fig. 9(c), it can be seen that using box or Scribble for interactive segmentation can effectively eliminate the uncertainty information generated during the interaction process, thereby obtaining a higher IoU. Furthermore, as shown in Fig. 9(b), each box position is calculated based on the deviation region between the previous predicted result and the ground truth mask. If the deviation region belongs to the foreground, the box is considered a positive prompt (red box), while if it belongs to the background, the box is considered a negative prompt (green box). This approach of using deviation-based box prompts achieves the goal of local refinement without increasing the model parameters.

D. Limitations and Future Perspectives

VPUFormer improves the efficiency and compatibility of existing pipelines. However, it still has the following limitations: Firstly, while we have unified three different visual interaction forms as user prompts in VPUFormer, there is open space to further investigate and incorporate more interaction forms in real-world applications, such as prompt masks, text information, and so on. Secondly, although we have alleviated the problem of object region ambiguity by selecting different interaction forms through increasing user input, the ambiguity still exists in a single interaction. As shown in Fig. 9, two people and the drum in front of them can all be separate target regions or combined as one foreground region. Thirdly, VPUFormer performs well across different benchmarks, these test sets and training sets belong to daily life scenes with small differences in data distribution. If we directly apply VPUFormer to medical images, as shown in Fig. 8, it needs to be fine-tuned on the target domain dataset; otherwise, the performance will decrease.

To address these limitations, in the future, we intend to further integrate other modalities of interactive types, such as

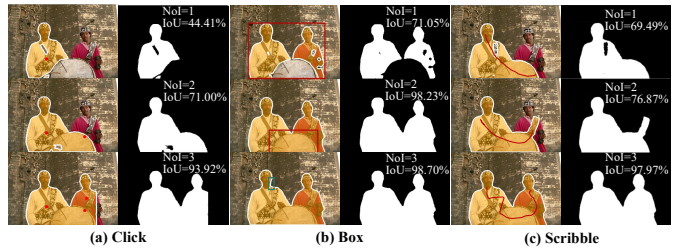


Fig. 9: Comparison of three different prompt types for interactive image segmentation.

text, voice, *etc.*, by utilizing the prompt encoder module to integrate different forms of user prompts. For the uncertainty problem caused by interactive input, [56], [57] focus on the issue of ambiguity and predict multiple potential results and let a selection network or the user choose from them. Building upon this, we aim to design a mechanism that gradually eliminates ambiguities by utilizing the added prompt information through user interaction. Additionally, cross-domain or open-set scenarios have been challenging and prominent research topics. By addressing the aforementioned issues, we can greatly enhance the performance of models in cross-domain or open-set data scenarios.

V. CONCLUSION

In this paper, we look into interactive image segmentation and propose VPUFormer, which adopts a novel encoding method (PuE) to effectively integrate diverse visual interaction forms as user prompts, flexibly switching between different visual interaction forms during the user interaction process to overcome the limitations of a single interaction form in practical applications. Then, we put forward the Dual-cross Merging Attention (DMA) to facilitate a more comprehensive interaction between image and prompt inputs. Additionally, we design the Prompt-to-Pixel Contrastive Loss (P²CL) to bring image semantic features closer to the features that are similar to the user prompt, while pushing away those image semantic features that are dissimilar to the user prompt features, by aligning the user prompt features with the corresponding pixel-level visual features to iteratively refine candidate semantic features. Extensive experiments on seven datasets with different backbone segmenters have demonstrated the superiority of our VPUFormer, setting the new state of the art.

REFERENCES

- [1] K. Yang, X. Hu, and R. Stiefelwagen, “Is context-aware CNN ready for the surroundings? Panoramic semantic segmentation in the wild,” *IEEE Trans. Image Process.*, vol. 30, pp. 1866–1881, 2021.
- [2] T. Wang, J. Yang, Z. Ji, and Q. Sun, “Probabilistic diffusion for interactive image segmentation,” *IEEE Trans. Image Process.*, vol. 28, no. 1, pp. 330–342, 2019.
- [3] G. Li *et al.*, “Personal fixations-based object segmentation with object localization and boundary preservation,” *IEEE Trans. Image Process.*, vol. 30, pp. 1461–1475, 2021.
- [4] H. Ding, H. Zhang, C. Liu, and X. Jiang, “Deep interactive image matting with feature propagation,” *IEEE Trans. Image Process.*, vol. 31, pp. 2421–2432, 2022.
- [5] J. Bai and X. Wu, “Error-tolerant scribbles based interactive image segmentation,” in *Proc. IEEE Conf. Comput. Vis. Pattern Recognit. (CVPR)*, 2014, pp. 392–399.

- [6] L. Grady, "Random walks for image segmentation," *IEEE Trans. Pattern Anal. Mach. Intell.*, vol. 28, no. 11, pp. 1768–1783, 2006.
- [7] Y. Li, J. Sun, C.-K. Tang, and H.-Y. Shum, "Lazy snapping," *ACM Trans. Graph. (TOG)*, vol. 23, no. 3, pp. 303–308, 2004.
- [8] X. Chen, Y. S. J. Cheung, S.-N. Lim, and H. Zhao, "Scribble-Seg: Scribble-based interactive image segmentation," *arXiv preprint arXiv:2303.11320*, 2023.
- [9] N. Xu, B. Price, S. Cohen, J. Yang, and T. S. Huang, "Deep interactive object selection," in *Proc. IEEE Conf. Comput. Vis. Pattern Recognit. (CVPR)*, 2016, pp. 373–381.
- [10] X. Chen, Z. Zhao, F. Yu, Y. Zhang, and M. Duan, "Conditional diffusion for interactive segmentation," in *Proc. IEEE Int. Conf. Comput. Vis. (ICCV)*, 2021, pp. 7345–7354.
- [11] Z. Lin, Z. Zhang, L.-Z. Chen, M.-M. Cheng, and S.-P. Lu, "Interactive image segmentation with first click attention," in *Proc. IEEE Conf. Comput. Vis. Pattern Recognit. (CVPR)*, 2020, pp. 13 339–13 348.
- [12] K. Sofiiuk, I. A. Petrov, and A. Konushin, "Reviving iterative training with mask guidance for interactive segmentation," in *Proc. IEEE Int. Conf. Image Process (ICIP)*, 2022, pp. 3141–3145.
- [13] J. Lin *et al.*, "AdaptiveClick: Clicks-aware transformer with adaptive focal loss for interactive image segmentation," *arXiv preprint arXiv:2305.04276*, 2023.
- [14] V. Lempitsky, P. Kohli, C. Rother, and T. Sharp, "Image segmentation with a bounding box prior," in *Proc. IEEE Int. Conf. Comput. Vis. (ICCV)*, 2009, pp. 277–284.
- [15] C. Rother, V. Kolmogorov, and A. Blake, "'GrabCut' interactive foreground extraction using iterated graph cuts," *ACM Trans. Graph. (TOG)*, vol. 23, no. 3, pp. 309–314, 2004.
- [16] J. Wu, Y. Zhao, J.-Y. Zhu, S. Luo, and Z. Tu, "MILCut: A sweeping line multiple instance learning paradigm for interactive image segmentation," in *Proc. IEEE Conf. Comput. Vis. Pattern Recognit. (CVPR)*, 2014, pp. 256–263.
- [17] A. Bearman, O. Russakovsky, V. Ferrari, and L. Fei-Fei, "What's the point: Semantic segmentation with point supervision," in *Proc. Eur. Conf. Comput. Vis. (ECCV)*, 2016, pp. 549–565.
- [18] R. Benenson, S. Popov, and V. Ferrari, "Large-scale interactive object segmentation with human annotators," in *Proc. IEEE Conf. Comput. Vis. Pattern Recognit. (CVPR)*, 2019, pp. 11 700–11 709.
- [19] A. Dosovitskiy *et al.*, "An image is worth 16x16 words: Transformers for image recognition at scale," in *Proc. Int. Conf. Learn. Represent. (ICLR)*, 2021.
- [20] K. He, X. Zhang, S. Ren, and J. Sun, "Deep residual learning for image recognition," in *Proc. IEEE Conf. Comput. Vis. Pattern Recognit. (CVPR)*, 2016, pp. 770–778.
- [21] K. Sun *et al.*, "High-resolution representations for labeling pixels and regions," *arXiv preprint arXiv:1904.04514*, 2019.
- [22] E. Xie, W. Wang, Z. Yu, A. Anandkumar, J. M. Alvarez, and P. Luo, "SegFormer: Simple and efficient design for semantic segmentation with transformers," *Proc. Adv. Neural Inf. Process. Syst. (NeurIPS)*, vol. 34, pp. 12 077–12 090, 2021.
- [23] T.-Y. Lin, P. Goyal, R. Girshick, K. He, and P. Dollár, "Focal loss for dense object detection," in *Proc. IEEE Int. Conf. Comput. Vis. (ICCV)*, 2017, pp. 2980–2988.
- [24] K. Sofiiuk, O. Barinova, and A. Konushin, "AdaptIS: Adaptive instance selection network," in *Proc. IEEE Int. Conf. Comput. Vis. (ICCV)*, 2019, pp. 7355–7363.
- [25] Y. Y. Boykov and M.-P. Jolly, "Interactive graph cuts for optimal boundary & region segmentation of objects in ND images," in *Proc. IEEE Int. Conf. Comput. Vis. (ICCV)*, vol. 1, 2001, pp. 105–112.
- [26] H. Yu, Y. Zhou, H. Qian, M. Xian, and S. Wang, "LooseCut: Interactive image segmentation with loosely bounded boxes," in *Proc. IEEE Int. Conf. Image Process (ICIP)*, 2017, pp. 3335–3339.
- [27] W.-D. Jang and C.-S. Kim, "Interactive image segmentation via back-propagating refinement scheme," in *Proc. IEEE Conf. Comput. Vis. Pattern Recognit. (CVPR)*, 2019, pp. 5297–5306.
- [28] K. Sofiiuk, I. A. Petrov, O. Barinova, and A. Konushin, "F-BRS: Rethinking backpropagating refinement for interactive segmentation," in *Proc. IEEE Conf. Comput. Vis. Pattern Recognit. (CVPR)*, 2020, pp. 8623–8632.
- [29] M. Forte, B. Price, S. Cohen, N. Xu, and F. Pitié, "Getting to 99% accuracy in interactive segmentation," *arXiv preprint arXiv:2003.07932*, 2020.
- [30] M. Zhou *et al.*, "Interactive segmentation as gaussian process classification," *arXiv preprint arXiv:2302.14578*, 2023.
- [31] B. Faizov, V. Shakhuro, and A. Konushin, "Interactive image segmentation with transformers," in *Proc. IEEE Int. Conf. Image Process (ICIP)*, 2022, pp. 1171–1175.
- [32] X. Chen, Z. Zhao, Y. Zhang, M. Duan, D. Qi, and H. Zhao, "FocalClick: Towards practical interactive image segmentation," in *Proc. IEEE Conf. Comput. Vis. Pattern Recognit. (CVPR)*, 2022, pp. 1300–1309.
- [33] Q. Wei, H. Zhang, and J.-H. Yong, "Focused and collaborative feedback integration for interactive image segmentation," *arXiv preprint arXiv:2303.11880*, 2023.
- [34] S. Zhang, J. H. Liew, Y. Wei, S. Wei, and Y. Zhao, "Interactive object segmentation with inside-outside guidance," in *Proc. IEEE Conf. Comput. Vis. Pattern Recognit. (CVPR)*, 2020, pp. 12 234–12 244.
- [35] H. Ding, S. Cohen, B. Price, and X. Jiang, "PhraseClick: Toward achieving flexible interactive segmentation by phrase and click," in *Proc. Eur. Conf. Comput. Vis. (ECCV)*, 2020, pp. 417–435.
- [36] A. Kirillov *et al.*, "Segment anything," *arXiv preprint arXiv:2304.02643*, 2023.
- [37] X. Zou *et al.*, "Segment everything everywhere all at once," *arXiv preprint arXiv:2304.06718*, 2023.
- [38] Z. Lin, Z.-P. Duan, Z. Zhang, C.-L. Guo, and M.-M. Cheng, "FocusCut: Diving into a focus view in interactive segmentation," in *Proc. IEEE Conf. Comput. Vis. Pattern Recognit. (CVPR)*, 2022, pp. 2637–2646.
- [39] Y. Xiong, Z. Zhou, Y. Dou, and Z. Su, "Gaussian vector: An efficient solution for facial landmark detection," in *Pro. Asi. Conf. Comput. Vis. (ACCV)*, 2020.
- [40] A. Vaswani *et al.*, "Attention is all you need," *Proc. Adv. Neural Inf. Process. Syst. (NeurIPS)*, vol. 30, 2017.
- [41] T.-Y. Lin, P. Dollár, R. Girshick, K. He, B. Hariharan, and S. Belongie, "Feature pyramid networks for object detection," in *Proc. IEEE Conf. Comput. Vis. Pattern Recognit. (CVPR)*, 2017, pp. 2117–2125.
- [42] F. Milletari, N. Navab, and S.-A. Ahmadi, "V-net: Fully convolutional neural networks for volumetric medical image segmentation," in *Proc. Int. Comput. on 3D Vis. (3DV)*, 2016, pp. 565–571.
- [43] D. Martin, C. Fowlkes, D. Tal, and J. Malik, "A database of human segmented natural images and its application to evaluating segmentation algorithms and measuring ecological statistics," in *Proc. IEEE Int. Conf. Comput. Vis. (ICCV)*, vol. 2, 2001, pp. 416–423.
- [44] B. Hariharan, P. Arbeláez, L. Bourdev, S. Maji, and J. Malik, "Semantic contours from inverse detectors," in *Proc. IEEE Int. Conf. Comput. Vis. (ICCV)*, 2011, pp. 991–998.
- [45] F. Perazzi, J. Pont-Tuset, B. McWilliams, L. Van Gool, M. Gross, and A. Sorkine-Hornung, "A benchmark dataset and evaluation methodology for video object segmentation," in *Proc. IEEE Conf. Comput. Vis. Pattern Recognit. (CVPR)*, 2016, pp. 724–732.
- [46] Y. Huang *et al.*, "InterFormer: Real-time interactive image segmentation," *arXiv preprint arXiv:2304.02942*, 2023.
- [47] Q. Liu, Z. Xu, G. Bertasius, and M. Niethammer, "SimpleClick: Interactive image segmentation with simple vision transformers," *arXiv preprint arXiv:2210.11006*, 2022.
- [48] T.-Y. Lin *et al.*, "Microsoft COCO: Common objects in context," in *Proc. Eur. Conf. Comput. Vis. (ECCV)*, 2014, pp. 740–755.
- [49] A. Gupta, P. Dollar, and R. Girshick, "LVIS: A dataset for large vocabulary instance segmentation," in *Proc. IEEE Conf. Comput. Vis. Pattern Recognit. (CVPR)*, 2019, pp. 5356–5364.
- [50] Z. Lin, Z. Zhang, L.-Z. Chen, M.-M. Cheng, and S.-P. Lu, "Interactive image segmentation with first click attention," in *Proc. IEEE Conf. Comput. Vis. Pattern Recognit. (CVPR)*, 2020, pp. 13 339–13 348.
- [51] S. Gerhard, J. Funke, J. Martel, A. Cardona, and R. Fetter, "Segmented anisotropic sstem dataset of neural tissue," *figshare*, pp. 0–0, 2013.
- [52] Q. Liu *et al.*, "PseudoClick: Interactive image segmentation with click imitation," in *Proc. Eur. Conf. Comput. Vis. (ECCV)*, 2022, pp. 728–745.
- [53] U. Baid *et al.*, "The RSNA-ASNR-MICCAI BraTS 2021 benchmark on brain tumor segmentation and radiogenomic classification," *arXiv preprint arXiv:2107.02314*, 2021.
- [54] F. Ambellan, A. Tack, M. Ehlke, and S. Zachow, "Automated segmentation of knee bone and cartilage combining statistical shape knowledge and convolutional neural networks: Data from the osteoarthritis initiative," *Med Image Anal.*, vol. 52, pp. 109–118, 2019.
- [55] L.-C. Chen, Y. Zhu, G. Papandreou, F. Schroff, and H. Adam, "Encoder-decoder with atrous separable convolution for semantic image segmentation," in *Proc. Eur. Conf. Comput. Vis. (ECCV)*, 2018, pp. 801–818.
- [56] Z. Li, Q. Chen, and V. Koltun, "Interactive image segmentation with latent diversity," in *Proc. IEEE Conf. Comput. Vis. Pattern Recognit. (CVPR)*, 2018, pp. 577–585.
- [57] J. H. Liew, S. Cohen, B. Price, L. Mai, S.-H. Ong, and J. Feng, "MultiSeg: Semantically meaningful, scale-diverse segmentations from minimal user input," in *Proc. IEEE Int. Conf. Comput. Vis. (ICCV)*, 2019, pp. 662–670.